Chemical Engineering Journal 437 (2022) 135255

Contents lists available at ScienceDirect

Chemical Engineering Journal

journal homepage: www.elsevier.com/locate/cej

Sponge-inspired sulfonated polyetheretherketone loaded with polydopamine-protected osthole nanoparticles and berberine enhances osteogenic activity and prevents implant-related infections

Shang Sang [a], Shengjie Wang [a], Chao Yang [a], Zhen Geng [b,*], Xianlong Zhang [a,*]

[a] Department of Orthopaedics, Shanghai Jiao Tong University, Affiliated Sixth People's Hospital, Shanghai, China
[b] Institute of Translational Medicine, Shanghai University, Shanghai 200444, China

ARTICLE INFO

Keywords:
Sulfonated polyetheretherketone
Osthole
Berberine
Osteogenesis
Antibacterial

ABSTRACT

Infection and loosening of implants after joint replacement are the complications that have troubled patients and doctors for a long time. To prevent such complications, we selected polyether ether ketone (PEEK) used in orthopedic implants and endowed it with antibacterial and osteogenic activities via surface modification. First, we made a spongy three-dimensional structure on the surface of PEEK via sulfonation reaction and then embedded osthole nanoparticles with osteogenic activity. In the process of material preparation, we creatively found that polydopamine (PDA) can protect the morphology of osthole nanoparticles. Then, we applied a silk fibroin–berberine coating with antibacterial function to the surface of the material. The covalent adsorption of silk fibroin on berberine realized rapid and sustained release of berberine from the material. *In vitro* experiments confirmed that (Ost + Ber)@SPEEK (sulfonated PEEK loaded with osthole particles and berberine) can promote osteogenesis by upregulating the expression of osteogenesis-related genes. Additionally, (Ost + Ber)@SPEEK prevents bacterial adhesion and has a killing effect on the suspended bacteria around it. The intrafemoral implant experiment in rats has confirmed that (Ost + Ber)@SPEEK can promote osteogenesis and prevent endophytic infection in vivo. This study presented a new strategy to fabricate biofunctionalized PEEK-based implants for potential applications in orthopedics field.

1. Introduction

For joint replacement surgery, implant infection and loosening are the most common and serious complications [1,2]. The loosening of the implant is caused by the lack of osteogenic activity of the inner implant and the lack of close combination with the surrounding bone tissue [3,4]. On the other hand, the main pathogen responsible for implant infection is *staphylococci* [5,6]. Statistically, the number of prosthesis revision operations due to internal plant infection and loosening increases yearly [7,8]. Revision surgery can be a huge traumatic blow to patients. Therefore, to avoid the occurrence of implant infection and loosening, it is necessary to develop an internal implant material that can promote osteogenesis and prevent staphylococcal infection. See (Scheme 1).

Recently, PEEK has been widely used in the manufacture of orthopedic implants because of its high mechanical strength as well as high temperature and radiation resistance [9,10]. However, the material itself has no antibacterial and osteogenic activities [11–14]. Therefore, the use of this material to make orthopedic implants cannot avoid the complications of prosthesis loosening and infection. In this study, we aim to modify the surface of PEEK material to promote its osteogenesis and antibacterial activities.

Osthole is an extract of Chinese herbal medicine Cnidium, which can promote osteogenesis by stimulating various osteogenic-related pathways [15,16]. So we believe that osthole can be loaded onto the surface of PEEK material to promote osteogenesis. However, the drug-loading capacity of the simple surface physical loading method is very limited. Inspired by the water absorption of the sponge stereo structure, we made a spongy–porous stereo structure on the surface of PEEK via sulfonation reaction to improve the loading capacity of PEEK for osthole [17]. Further, the osthole particles prepared via reverse deposition were loaded into the porous structure, which increased the drug-loading capacity of the materials. Interestingly, we found that without the protection of polydopamine (PDA), osthole nanoparticles in its water

* Corresponding authors at: Institute of Translational Medicine, Shanghai University, Shanghai 200444, China.
E-mail addresses: nanboshan1987@163.com (Z. Geng), dr_zhangxianlong@sjtu.edu.cn (X. Zhang).

https://doi.org/10.1016/j.cej.2022.135255
Received 11 January 2022; Received in revised form 8 February 2022; Accepted 10 February 2022
Available online 12 February 2022

suspension would turn into osthole crystallization when dried. By contrast, after co-incubating with dopamine (DA) in an alkaline condition for a particular period of time, the PDA film formed on the surface of the osthole nanoparticles will hinder the formation of osthole crystallization, resulting in PDA-osthole nanoparticles with uniform morphology. In addition, we realized a long-term stable release of osthole from sulfonated PEEK loaded with osthole particles using the characteristics of osthole's low solubility in water [18]. Moreover, the effective concentration of osthole in promoting osteogenesis is close to its saturated concentration in water [16,19]. By this way, the sulfonated PEEK material loaded with osthole particles can achieve a lasting osteogenic activity.

Berberine is extracted from the roots of Coptis chinensis, a Chinese herbal medicine [20]. This drug can effectively kill staphylococci by interfering with bacterial DNA replication and protein synthesis [21,22]. So we chose berberine to endow antibacterial activity to PEEK materials. However, the simple physical loading of berberine is limited, and owing to the high solubility of berberine in water, the physical loading cannot avoid the explosive release of berberine from the initial material. Thus, the controllable release of berberine cannot be realized. Therefore, we selected carboxyl-functional-groups rich silk fibroin and used the covalent adsorption of the carboxyl group to berberine for increasing the loading amount of berberine on PEEK and realize its sustained and rapid release [23]. Using this method, we have endowed PEEK with excellent antibacterial ability.

Based on the above, we prepared (Ost + Ber)@SPEEK, and this material can realize the controllable release of osthole and berberine. To investigate the osteogenic and antibacterial functions of (Ost + Ber)@SPEEK, we performed comprehensive *in vitro* and in vivo experiments and found that (Ost + Ber)@SPEEK promoted osteogenic activity and prevented staphylococcus-related infections.

2. Experimental section

2.1. Preparation of osthole nanoparticles–water suspension, osthole crystallization, PDA-osthole nanoparticles, PDA microspheres containing osthole nanoparticles and PDA-osthole nanoparticles loaded SPEEK

Firstly, a 10 mg/ml osthole (purchased from Qing lan biotech CO., LTD) solution in 100% alcohol was prepared and added to deionized water at a 1:10 vol ratio to generate a 1 mg/ml osthole nanoparticles–water suspension. Then the osthole nanoparticles–water

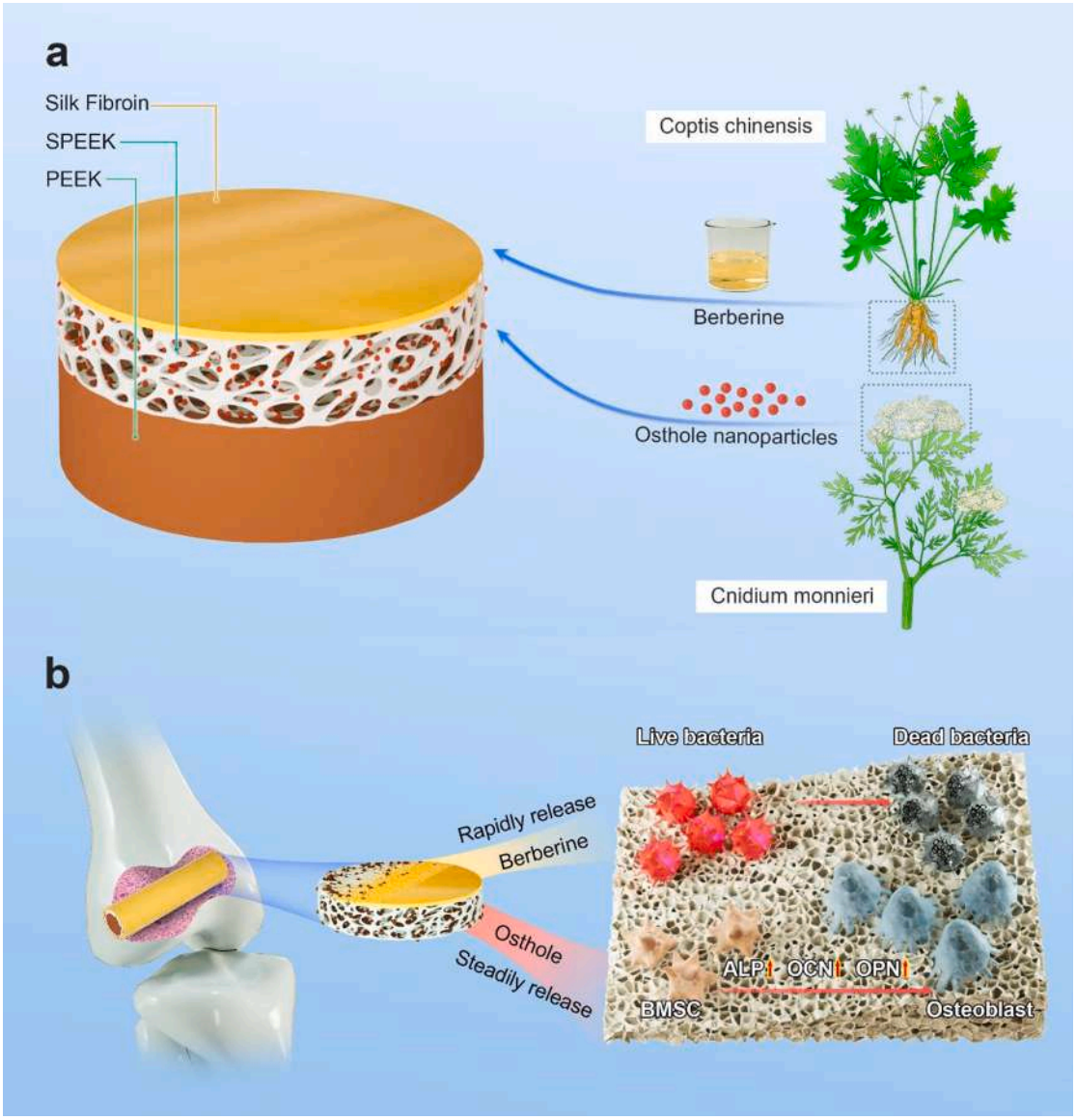

Scheme 1. (a). The composition of (Ost + Ber)@SPEEK. (b). The antibacterial and osteogenic functions of (Ost + Ber)@SPEEK.

suspension was divided into three groups. In group one, the osthole nanoparticles–water suspension was dried directly at room temperature, and the osthole crystallization was obtained. In group two, 2 mg/ml DA was added to the osthole nanoparticles–water suspension and the pH was adjusted to 8.5 using the Tris buffer. Next, the suspension was placed at room temperature for 18 h. Then the PDA-osthole particles were obtained after drying the suspension. In group three, the 2 mg/ml DA was added to the osthole nanoparticles–water suspension and the pH was adjusted to 8.5 using the Tris buffer. The suspension was placed at room temperature for 36 h. After the suspension was dried, PDA microspheres containing osthole nanoparticles were obtained.

PEEK raw materials were purchased from GEHR Co., Germany. Then PEEK raw materials were processed as wafers (diameter: 1 cm, thickness: 1 mm) and rods (diameter: 2 mm, length: 1 cm). Both were separately placed into beakers where sulfonation reactions were conducted by adding concentrated sulfuric acid (98%) at room temperature. The solutions were stirred, with groups reacting at 7 min and 14 min respectively, and the products were labeled SP1 and SP2. Then, SPEEK wafers and rods were washed repeatedly in deionized water, incubated at 120 °C for 4 h to remove residual sulfur, and dried at room temperature.

Wafer and rod-shaped SP1 and SP2 materials were placed into a beaker and osthole nanoparticles–water suspension (1 mg/ml) was added. Then 2 mg/ml DA was added to the suspension and the pH was adjusted to 8.5 using the Tris buffer. The beaker was agitated at 50 rpm for 20 h. Then all of the materials were rinsed three times in deionized water and Ost@SP1 (SP1 loaded with PDA-osthole nanoparticles) and Ost@SP2 (SP2 loaded with PDA-osthole nanoparticles) were generated. The materials were then dried at room temperature.

2.2. Preparation of (Ost + Ber)@SP1 and (Ost + Ber)@SP2

Silk fibroin was extracted according to a standard method [24]. The mass fraction of silk fibroin solution was adjusted to 5% and evenly applied to Ost@SP1 and Ost@SP2 materials. For wafer-shaped materials, each side was covered with 10 μl silk fibroin solution, dried at room temperature, and repeated twice. For rod-shaped materials, 5 μl silk fibroin solution (5%) was applied, dried at room temperature, and repeated twice. Materials coated with silk fibroin were immersed in 1 mg/ml berberine (purchased from Sangon Biotech (Shanghai) Co., Ltd) aqueous solution for 5 min and dried at room temperature to generate (Ost + Ber)@SP1 and (Ost + Ber)@SP2 materials.

2.3. Characterization of materials

A Malvern Zetasizer Nano ZS90 was used to assess particle size of osthole nanoparticles in osthole nanoparticles-water suspensions. Then, osthole crystallization, PDA-osthole nanoparticles and PDA microspheres containing osthole nanoparticles were observed by scanning electron microscopy (SEM) (Zeiss Gemini 300). Energy dispersive spectrometer (EDS) was used to analyze the elemental content of osthole crystallization, PDA-osthole nanoparticles and PDA microspheres containing osthole nanoparticles. Diameter and thickness dimensions of wafer-shaped PEEK, SP1 and SP2 materials and diameter of rod-shaped PEEK, SP1 and SP2 materials were measured using a Vernier calipers. SP1 and SP2 morphologies were observed using SEM and surface pore sizes were measured and counted.

SEM was used to observe (Ost + Ber)@SP1 and (Ost + Ber)@SP2 materials and EDS used to analyze the elemental content of each group. A contact angle measuring instrument (OCA25) was used to measure the static contact angles of PEEK, SP1, SP2, (Ost + Ber)@SP1, and (Ost + Ber)@SP2.

Berberine release experiments: each (Ost + Ber)@SP1 and (Ost + Ber)@SP2 wafer was immersed in 1 ml deionized water; the extract was collected at 4 h, 12 h, 24 h, 48 h, 48 h, and 72 h and the solution was changed with deionized water at the same time. The absorbance at 420 nm for each time point extract was measured using a spectrophotometer; the concentration of berberine was calculated based on absorbance. All materials were photographed before and after the release experiments.

Osthole release experiments: each (Ost + Ber)@SP1 and (Ost + Ber)@SP2 wafer was soaked in 1 ml deionized water. Extracts were collected and exchanged with water on day 1, 4, 7, 10, 13, 16, 19, 22, 25, and 28. The absorbance at 200 nm for each time point extract was measured via ultraviolet spectrophotometry and concentrations of osthole were calculated according to absorbance. (Ost + Ber)@SP1 and (Ost + Ber)@SP2 after osthole release experiments were collected, dried, and observed using SEM.

2.4. Cell compatibility experiments

rBMSCs were extracted according to standard methods and cultured in MEM medium supplemented with 10% fetal bovine serum (FBS) [25]. Sterilized wafer-like PEEK, SP1, SP2, (Ost + Ber)@SP1, and (Ost + Ber)@SP2 were equally divided into five groups; each group contained three pieces of material, one piece per well in a 24-well plate. Then, 0.5 ml of 1×10^5 rBMSCs cells/ml in MEM medium supplemented with 10% fetal bovine serum were added to each well. At the meanwhile, pick another five groups of sterilized wafer-like PEEK, SP1, SP2, (Ost + Ber)@SP1, and (Ost + Ber)@SP2 and each group contained three pieces of material. Put these matreials one piece per well in a 24-well plate. Then, 0.5 ml MEM medium supplemented with 10% fetal bovine serum were added to each well and name these groups as control groups without cells. After incubation at 37 °C for 24 h, 50 μl Cell Counting Kit-8 (CCK-8) solution was added to each well and further incubated for 1 h. Then, the absorbance was recorded at 450 nm using spectrophotometry (The final absorbance is the absorbance of the cell-containing group minus the absorbance of the corresponding control group without cells). Then, all materials were removed, washed thrice in phosphate buffered saline (PBS), fixed by with 2.5% glutaraldehyde and dehydrated via standard methods, and then cell adhesion on surfaces was examined using SEM after spraying with gold. The cells adhering to the culture plate were stained with a live–dead staining kit (Shanghai Maokang Biotechnology Co.,Ltd.) and photographed using a fluorescence microscope (Leica).

rBMSCs were cultured as described. Then, sterilized wafer-like PEEK, SP1, SP2, (Ost + Ber)@SP1, and (Ost + Ber)@SP2 materials were equally divided into five groups; each group contained three pieces of material, one piece per well in a 24-well plate. Then, 0.5 ml of 1×10^5 rBMSCs cells/ml in a-MEM supplemented with 10% FBS were added to each well. At the meanwhile, prepare the control groups without cells as described above. Plates were incubated at 37 °C and the medium of the cells was changed by a-MEM supplemented with 10% FBS on the third day. After incubation at 37 °C for 4 days, 50 μl CCK-8 solution was added to each well and further incubated at for 1 h. Then, the absorbance at 450 nm was measured and calculated as described above. Then, all materials were removed, washed thrice in PBS, fixed by with 2.5% glutaraldehyde and dehydrated via standard methods, and then cell adhesion on the surface was examined using SEM after spraying with gold. The cells adhering to the culture plate were stained with a live–dead staining kit (Shanghai Maokang Biotechnology Co.,Ltd.) and photographed using a fluorescence microscope (Leica).

2.5. In vitro osteogenic experiments

Disinfect wafer-shaped PEEK, SP1, SP2, (Ost + Ber)@SP1 and (Ost + Ber)@SP2. Three pieces of materials were taken from each group. Then one piece of material soaked in 1 ml osteogenic medium (Cyagen Biosciences Co., USA) respectively. On day 1, 4, 7, 10, 13, 16, and 19, extracts were collected and use osteogenic medium exchange fluid.

Two hundred microliter (200 μl) cell suspensions containing 10^5/ml cells was planted in a 48-well plate and divided into five groups. Use each group of extract collected in former procedure change the medium of each group of cells for the first day, 4 days, 7 days, 10 days, 13 days,

16 days and 19 days. Then, a part of cells from each group were fixed by 4% paraformaldehyde on days 7 and 14, stained with alkaline phosphatase (ALP), and photographed. An ALP activity kit (Beyotime Biotechnology) was used to test ALP activities in groups. At the same time point, another batch of cells cultured under the same conditions were fixed by 4% paraformaldehyde, permeabilized with 0.1% Triton-X for 30 min, blocked with 1% BSA for 1 h in room temperature, and incubated with ALP or Osteocalcin (OCN) primary antibodies (Affinity Biosciences) overnight at 4 °C. Subsequently, ALP or OCN secondary antibodies (Affinity Biosciences) were applied to attach to the primary antibodies. At last, phalloidin and DAPI were used to stain the cytoskeleton and nuclei respectively. A fluorescence microscope (Leica) was used to acquire representative images.

Cells from each group were also collected on day 14 after which RNA was extracted using TRIzol and complementary DNA was synthesized using a RevertAid First Strand cDNA synthesis kit. Quantitative gene analyses were conducted using the FastStart Universal SYBR Green Master Mix on a PCR instrument. The $2^{-\triangle\triangle}$Ct method was used to compare mRNA expression between the groups. PCR primers are shown in Table S1. GAPDH was used as a housekeeping gene.

Other cells were grown to 21 days fixed by 4% paraformaldehyde, stained with alizarin red and photographed. After alizarin red was released by cetylpyridine, the absorbance of each group was measured at 562 nm.

2.6. In vitro antibacterial experiments

Staphylococcus aureus (*S. aureus*) and Staphylococcus epidermidis (*S. epidermidis*) was purchased from Shanghai Luwei Technology Co., Shanghai, China. Wafer-shaped PEEK, SP1, SP2, (Ost + Ber)@SP1, and (Ost + Ber)@SP2 were disinfected. Three pieces of materials from each group were placed on blood agar plates preinoculated with *S. aureus* and cultured for 24 h at 37 °C. Another three pieces materials from each group were placed on blood agar plates preinoculated with S. *epidermidis* and cultured for 24 h at 37 °C. Bacteriostatic ring were observed and photographed the next day.

Six PEEK wafers, SPEEK wafers, SP1 wafers, SP2 wafers, (Ost + Ber) @SP1 wafers, and (Ost + Ber)@SP2 wafers were disinfected and placed in 24-well plates. Next, 100 μl *S. aureus* or S. *epidermidis* (1×10^6 CFU/ml) was dropped onto the sample surface with a microsyringe and cultured at 37 °C for 24 h. Three wafers from each group were then rinsed thrice in PBS to remove unadherent surface bacteria and placed in 1 ml PBS for ultrasonication for 5 min. The bacterial solution was then serially diluted, inoculated onto Mueller-Hinton agar (MH) plates, and incubated for 24 h. The next day, colonies on MH plates of each group were counted and the content of bacteria in the shaking solution of each group was statistically analyzed. Another three wafers in each group were rinsed thrice in PBS, fixed in 2.5% glutaraldehyde, and dehydrated via standard methods. After spraying with gold, adhesive bacteria on materials of each group were observed using SEM.

Three PEEK wafers, SP1 wafers, SP2 wafers, (Ost + Ber)@SP1 wafers, and (Ost + Ber)@SP2 wafers in each group were sterilized and placed in a 24-well plate. Then, 500 μl *S. aureus* or S. *epidermidis* at 1×10^6 CFU/ml was added to each well and incubated for 24 h at 37 °C. After this, 100 μl bacterial solution from each group was serially diluted, inoculated onto MH plates, and incubated for 24 h. Colonies on MH plates of each group were recorded and the contents of bacteria in the suspension of each group were statistically analyzed.

2.7. In vivo osteogenic experiments

The animal experiments were approved by the Animal Care Committee of Shanghai Jiao Tong University Affiliated Sixth People's Hospital. And all the operations on animals strictly conform to the policies of the Institutional Animal Care and Use Committee of Shanghai Jiaotong University affiliated Shanghai sixth people's hospital. Six PEEK rods, SP1 rods, SP2 rods, (Ost + Ber)@SP1 rods, and (Ost + Ber)@SP2 rods were disinfected. Thirty 8-week-old Sprague–Dawley (SD) rats were divided into five groups with six rats per group. After applying standard anesthesia, the knee joint was disinfected, an oblique incision was made on the side, soft tissue separated, and the femoral condyle was exposed. A sterile 2 mm diameter drill bit was used to make a hole in the midpoint of the femoral condyle. And PEEK rods, SP1 rods, SP2 rods, (Ost + Ber) @SP1 rods, and (Ost + Ber)@SP2 rods were placed into the drilled holes (one for each), the wound was sutured after disinfection. Rats fed by routine methods. At the end of 4th week after surgery, rats were intraperitoneally injected with calcein dyes (20 mg/kg). At the end of 5th week, three rats in each group were selected and femurs on the operative side were harvested. After the soft tissue around the knee joint was removed, micro CT scanning was performed to observe and calculate trabecular thickness (Tb.Th), trabecular number (Tb.N), percent bone volume (BV/TV), and bone mineral density (BMD) of new bone around implants of each group. At the 8th week, each rat was intraperitoneally injected with alizarin red (30 mg/kg). At the 10th week, the femurs on the operative side of the remaining three rats in each group were harvested, and after soft tissue around the knee joint was removed, micro CT scanning was performed again to observe and calculate Tb.Th, Tb.N, BV/TV, BMD of new bone around implants of each group. Femurs at the 10th week were fixed, dehydrated, embedded, and then sliced (200 μm sections) along the coronal section of the femur (perpendicular to the implanted rod). The newly formed bone around implants of each group was observed using fluorescence confocal microscopy. Emission wavelengths were 488 nm and 560 nm. Then, tissue sections were stained with Van Gieson (VG) and the distribution of bone collagen around implants of each group was observed and photographed.

2.8. In vivo antibacterial experiments

Three PEEK rods, SP1 rods, SP2 rods, (Ost + Ber)@SP1 rods, and (Ost + Ber)@SP2 rods were disinfected. Fifteen 8-week-old SD rats were divided into five groups, with three rats per group. After standard anesthesia, the knee joint was disinfected, an oblique incision made on the lateral side of the knee joint, soft tissue separated, and the femoral condyle exposed. A sterile 2 mm diameter drill bit was used to make a hole in the midpoint of the femoral condyle. Then, 20 μl *S. aureus* (10^6 CFU/ml) was injected into each hole and the prepared materials were placed into drilled holes (one for each hole). Then wounds were sutured. Rats fed by routine methods. During the 2nd week, rats were anesthetized and MRI (CG NOVILA 7.0 T, Shanghai Chenguang Medical Technologies Co., LTD) was performed on these operated femurs; T2 weighted imaging was used to observe edema around implants. Rats were kept until the 5th week, after which femurs on the operative side were harvested and femoral condyles were photographed. After weighing, a part of the tissue around implanted rods from each group was broken by tissue homogenizer, then the homogenized tissue of each group was serially diluted by normal saline and spread on MH plates for colony counting. After the coated culture plate was cultured in 37 °C incubator for 1 day, colonies were counted and bacterial content in tissues of each group was calculated.

The next, micro CT examinations were performed on these femoral condyles to observe bone tissue around implants, with three-dimension (3D) reconstructions performed on each group of femoral condyles to further observe bone destruction around. Then all femurs were fixed by paraformaldehyde and then decalcified by ethylenediaminetetraacetic acid decalcification solution. Next these decalcified femurs were sliced (5 μm sections) along the coronal section of the femur and stained with hematoxylin & eosin (HE) and Giemsa. Finally, the sections were observed by a microscope to display the inflammatory tissue proliferation and bacteria colony distribution around implants of each group.

2.9. Statistical analysis

In this paper, the data were presented as the mean ± standard deviation. Differences among groups were analyzed by Student's *t* test and ANOVA using Prism 8 (GraphPad Software). $P < 0.05$ was considered a significant difference.

3. Results

3.1. Characterization of osthole nanoparticles–water suspension, osthole crystallization, PDA-osthole nanoparticles, and PDA microspheres loaded with osthole nanoparticles, SP1, SP2, Ost@SP1, and Ost@SP2

The general process for producing osthole crystallization, osthole nanoparticles, and PDA microspheres loaded with osthole nanoparticles and SPEEK loaded with PDA-osthole nanoparticles was shown in Fig. 1a. The particle size distribution of osthole nanoparticles in suspension is shown in Fig. 1b; the average particle size was 500–700 nm. The SEM image and elemental distribution of carbon, nitrogen, and oxygen (C, O, N) in osthole crystallization are shown in Fig. 1c. It is evident that osthole nanoparticles in suspension will crystallize into large pieces if dried without the protection of PDA. Furthermore, the length and width of these crystallizations are substantially larger than 10 um.

Fig. 1d shows the SEM image as well as the elemental distribution of C, O, and N in PDA-osthole nanoparticles. This image shows that after 18 h of the reaction, a thin PDA coating forms on the surface of the osthole nanoparticles. Moreover, the coating hinders the crystallization of ostholes during drying. Resultantly, the size of PDA-osthole nanoparticles obtained by incubating osthole nanoparticles with DA in an alkaline environment for 18 h is extremely close to that of osthole nanoparticles in osthole aqueous suspension. We also showed the SEM images of osthole raw materials and PDA-osthole nanoparticles in Fig. S1 to highlight the difference between the morphology of them. The size of PDA microspheres containing osthole nanoparticles obtained by incubating osthole nanoparticles with DA in an alkaline environment for 36 h is mainly distributed in the range of 1–1.5 um. (Fig. 1e). The EDS spectra and the quantitative analysis results of osthole crystallization, osthole nanoparticles, and PDA microspheres containing osthole nanoparticles were shown in Fig. S2-4. Fig. 1f shows SEM images of PEEK reacting with concentrated sulfuric acid at 7 min (SP1) and PEEK reacting with concentrated sulfuric acid at 14 min (SP2). The SP2 pore diameter (the average pore diameter was 1.2–1.7 um) was significantly larger than SP1 (the average pore diameter was 500–800 nm), and the number of SP2 holes was significantly higher than SP1 (Fig. S5). According to the above experimental data, it is evident that only the PDA-osthole nanoparticles obtained by incubating osthole nanoparticles with DA for 18 h are suitable to be loaded into SPEEK materials, especially SP2. It should be emphasized that differences between SP1 and SP2 were only evident in surface microstructures. The measurement and statistics of the size of wafer-shaped and rod-shaped PEEK, SP1, and SP2 are shown in Fig. S6–10, demonstrating that there is no difference in the macroscopic size of the three materials. Furthermore, the majority of the

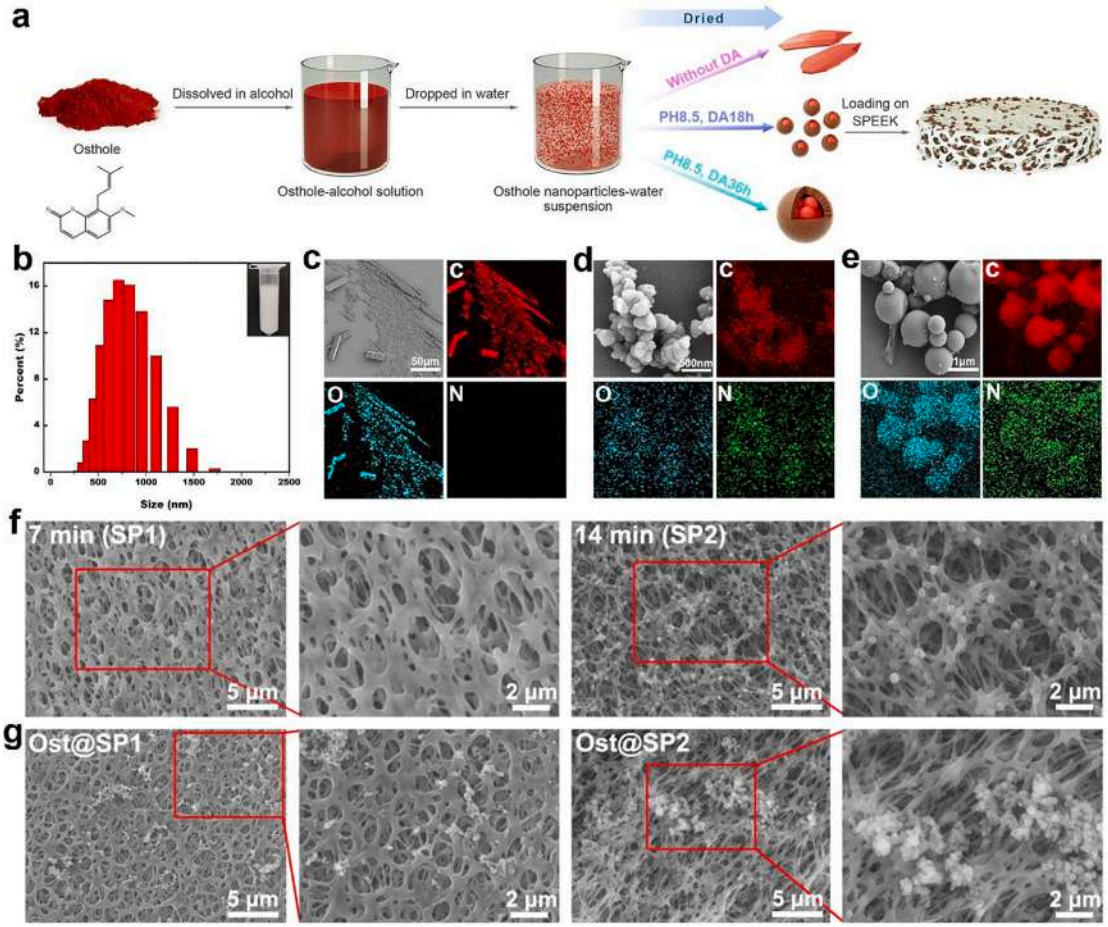

Fig. 1. Osthole crystallization, osthole nanoparticles, and PDA microspheres loaded with osthole nanoparticles, SP1, SP2, Ost@SP1, and Ost@SP2: (a) The general process of the preparation of osthole crystallization, osthole nanoparticles, and PDA microspheres loaded with osthole nanoparticles and SPEEK loaded with PDA-osthole nanoparticles; (b) Particle size statistics of osthole-water suspension (Upper right corner: picture of osthole nanoparticles-water suspension); (c) SEM image and elemental mapping of osthole crystallization; (d) SEM image and elemental mapping of PDA-osthole nanoparticles; (e) SEM image and elemental mapping of PDA microspheres containing osthole nanoparticles; (f) Elemental distribution results using EDS (e) SEM images of SP1 and SP2 (g) SEM images of Ost@SP1 and Ost@SP2.

PDA-osthole nanoparticles were deposited on the surface of Ost@SP1, whereas the particles on Ost@SP2 were deposited interiorly (Fig. 1g). Thus, PDA-osthole nanoparticles deposited on Ost@SP2 were significantly higher per unit area than the PDA-osthole nanoparticles deposited on Ost@SP1.

3.2. Characterization of (Ost + Ber)@SP1 and (Ost + Ber)@SP2

SEM images of (Ost + Ber)@SP1 and (Ost + Ber)@SP2 are shown (Fig. 2a); the surfaces of both materials were relatively flat with a small numbers of protuberances. The distribution of elements on (Ost + Ber)@SP1 and (Ost + Ber)@SP2 surfaces was also investigated (Fig. 2b); C, O, and N distributions on both materials were relatively uniform. We also collected images of (Ost + Ber)@SP1 and (Ost + Ber)@SP2 before and after the berberine release experiments (Fig. 2c). The surfaces of both materials were uniformly yellow before release, indicating that berberine was uniformly loaded on the surface. After release experiments, the yellow color on surfaces of both materials became lighter, suggesting the release of berberine. Note that after the release, the surface of both materials remained light brown yellow, indicating that low levels berberine remained on the surface after 72 h and suggesting that silk fibroin had a strong adsorption potential for berberine. Fig. 2f shows berberine release curves, and Fig. S11 shows images of extracts of (Ost + Ber)@SP1 and (Ost + Ber)@SP2 groups at different times. Berberine release from materials was rapid in the first 4 h, because initially, the material had a certain level of physical adsorption for berberine. In the following 72 h, berberine release was relatively stable, reflecting the chemical adsorption effects of silk fibroin for berberine. Fig. 2d shows the SEM images of (Ost + Ber)@SP1 and (Ost + Ber)@SP2 after drug release. After 4 weeks of release testing, almost no residual osthole nanoparticles on (Ost + Ber)@SP1 were observed, whereas many osthole nanoparticles were "embedded" in (Ost + Ber)@SP2. This indicated that spongy SP2 was more efficient in loading osthole nanoparticles. Release curves for osthole was also generated (Fig. 2g). The sustained release curve also showed that (Ost + Ber)@SP1 maintained a stable osthole release in the first week, whereas the osthole release in (Ost + Ber)@SP1 decreased gradually after 1 week. In contrast, (Ost + Ber)@SP2 stably released osthole in the 4-week release test, further indicating that spongy (Ost + Ber)@SP2 had a larger and more stable load on osthole.

Fig. 2e shows the contact angles of the five materials; those for (Ost + Ber)@SP1 and (Ost + Ber)@SP2 were smaller than PEEK, SP1, and

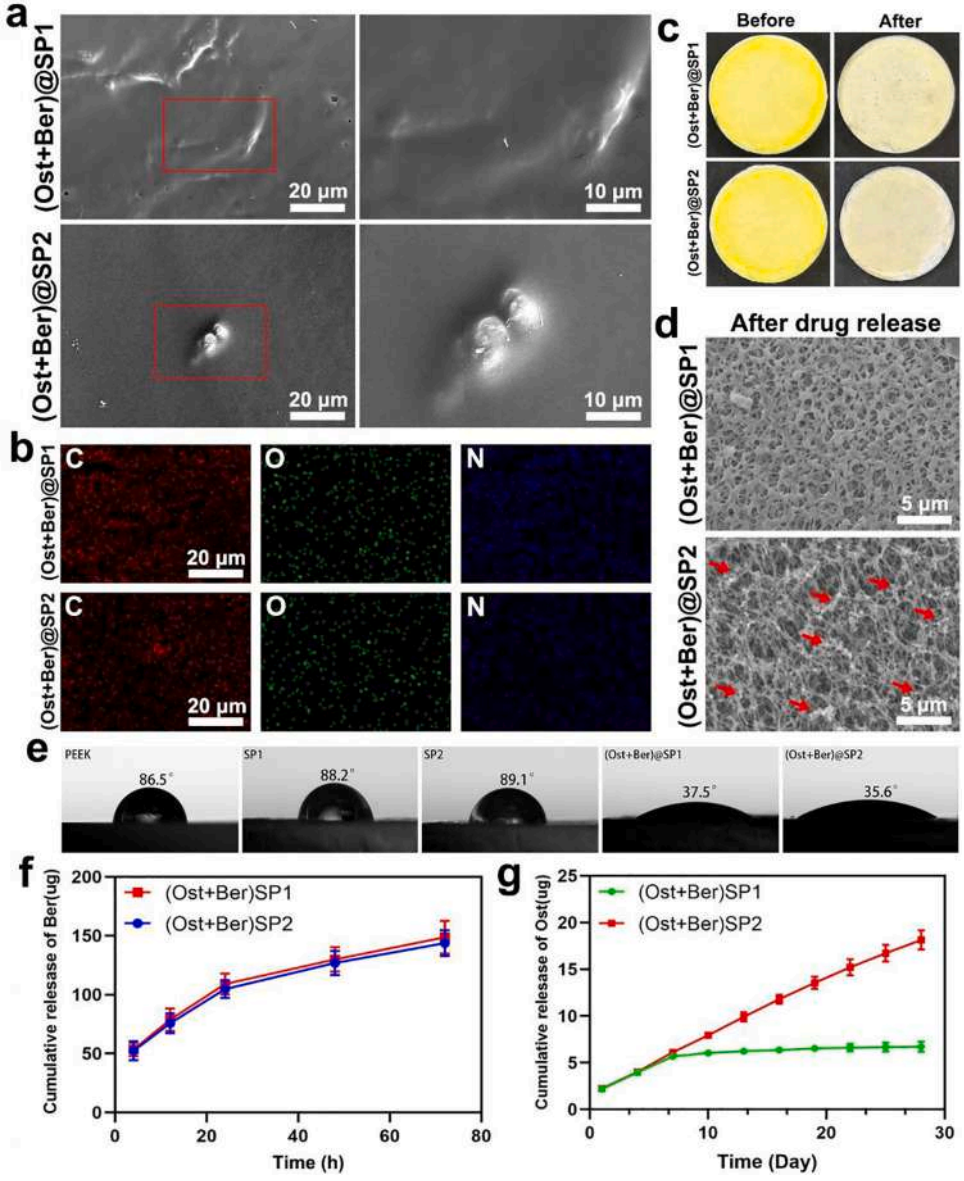

Fig. 2. Characterization of (Ost + Ber)@SP1 and (Ost + Ber)@SP2. (a). SEM images of (Ost + Ber)@SP1 and (Ost + Ber)@SP2. (b). Elemental distribution data for (Ost + Ber)@SP1 and (Ost + Ber)@SP2 by EDS. (c). Photos of (Ost + Ber)@SP1 and (Ost + Ber)@SP2 before and after berberine release experiments. (d). SEM images of (Ost + Ber)@SP1 and (Ost + Ber)@SP2 after osthole release experiments. The red arrow indicates osthole nanoparticles in the interior of (Ost + Ber)@SP2. (e). Contact angles for the five groups of materials. (f). Berberine release curves of (Ost + Ber)@SP1 and (Ost + Ber)@SP2. (g) Osthole release curves of (Ost + Ber)@SP1 and (Ost + Ber)@SP2.

SP2. Smaller contact angles meant improved hydrophilicity, which is beneficial for the adsorption of water-soluble drugs; statistical results of contact angle are shown in Fig. S12.

3.3. Cell compatibility experiments

SEM images of rBMSCs adhesion to materials at day 1 and day 4 after seeding are shown in Fig. 3a; rBMSCs adhered and grew well on all materials. The live/dead staining of rBMSCs at day 1 and day 4 (Fig. 3b) after seeding also indicated that rBMSCs grew well around all materials. CCK-8 data on the 1st day are also shown (Fig. 3c) and confirmed cell viability on materials was good, with no significant differences in cell viability between groups. CCK-8 data on the 4th day indicated that cell viability was good (Fig. 3d), and when compared with CCK-8 data from day 1, viability appeared enhanced, suggesting that cells were proliferating well on and around all materials.

3.4. In vitro osteogenic experiments

ALP immunofluorescence staining of cells staining after 7 days culture (Fig. 4a) showed that ALP fluorescence in (Ost + Ber)@SP1 and (Ost + Ber)@SP2 groups was significantly stronger than the other groups. The statistical analysis of ALP immunofluorescence intensity per cell of the five groups (Fig. 4b) also confirmed this result. ALP staining of the five groups of cells on the 7th day of culture (Fig. 4c) showed that staining in (Ost + Ber)@SP1 and (Ost + Ber)@SP2 groups was significantly stronger than the other groups. And the statistics of ALP activity data (Fig. 4d) in the five groups confirmed this result. ALP staining of five groups of cells after 14 days culture (Fig. 4e) showed that the staining in the (Ost + Ber)@SP1 and (Ost + Ber)@SP2 groups were significantly higher than the other three groups, whereas they were significantly higher in the (Ost + Ber)@SP2 group than in the (Ost + Ber)@SP1 group.

OCN immunofluorescence staining of cells staining after 14 days culture (Fig. 5a) showed that OCN fluorescence in (Ost + Ber)@SP1 and (Ost + Ber)@SP2 groups was significantly stronger than the other groups, whereas they were significantly higher in the (Ost + Ber)@SP2 group than in the (Ost + Ber)@SP1 group. The statistical analysis of OCN immunofluorescence intensity per cell of the five groups (Fig. 5b) also confirmed this result. Alizarin red staining in groups at 21 days (Fig. 5c) showed that calcium nodule numbers and areas in (Ost + Ber) @SP1 and (Ost + Ber)@SP2 groups were significantly higher than the

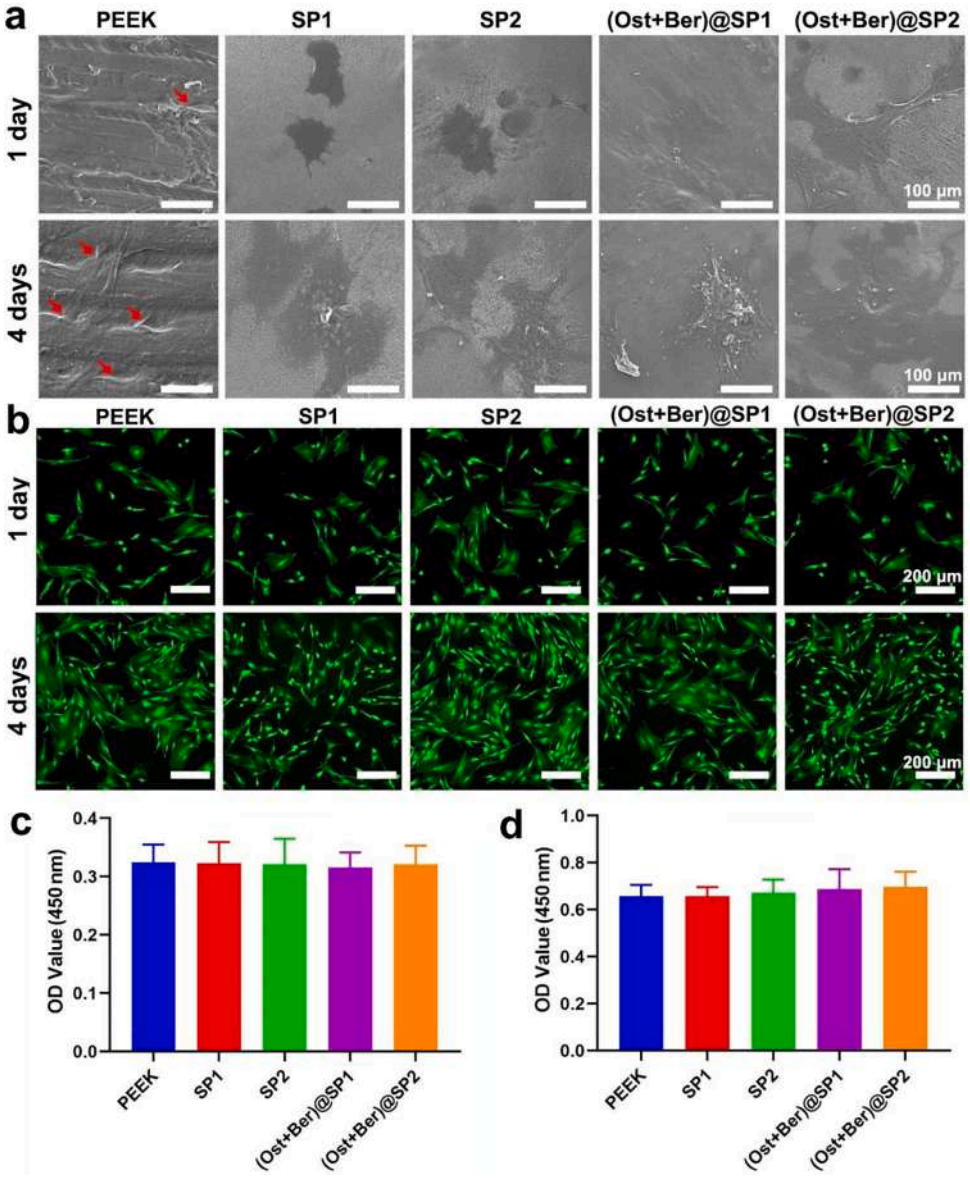

Fig. 3. Cell compatibility assays. (a). SEM images of (rBMSCs) adhesion on the surface of materials on the 1st and 4th day after seeding; red arrows indicate rBMSCs. (b). Fluorescence images of rBMSCs co-cultured with different groups of materials on the 1st and 4th day after seeding (Green indicates live rBMSCs and red indicates dead rBMSCs). (c). CCK-8 experiment results of rBMSCs co-cultured with five kinds of materials on the 1st day (d). CCK-8 experiment results of rBMSCs co-cultured with five kinds of materials on the 4th day.

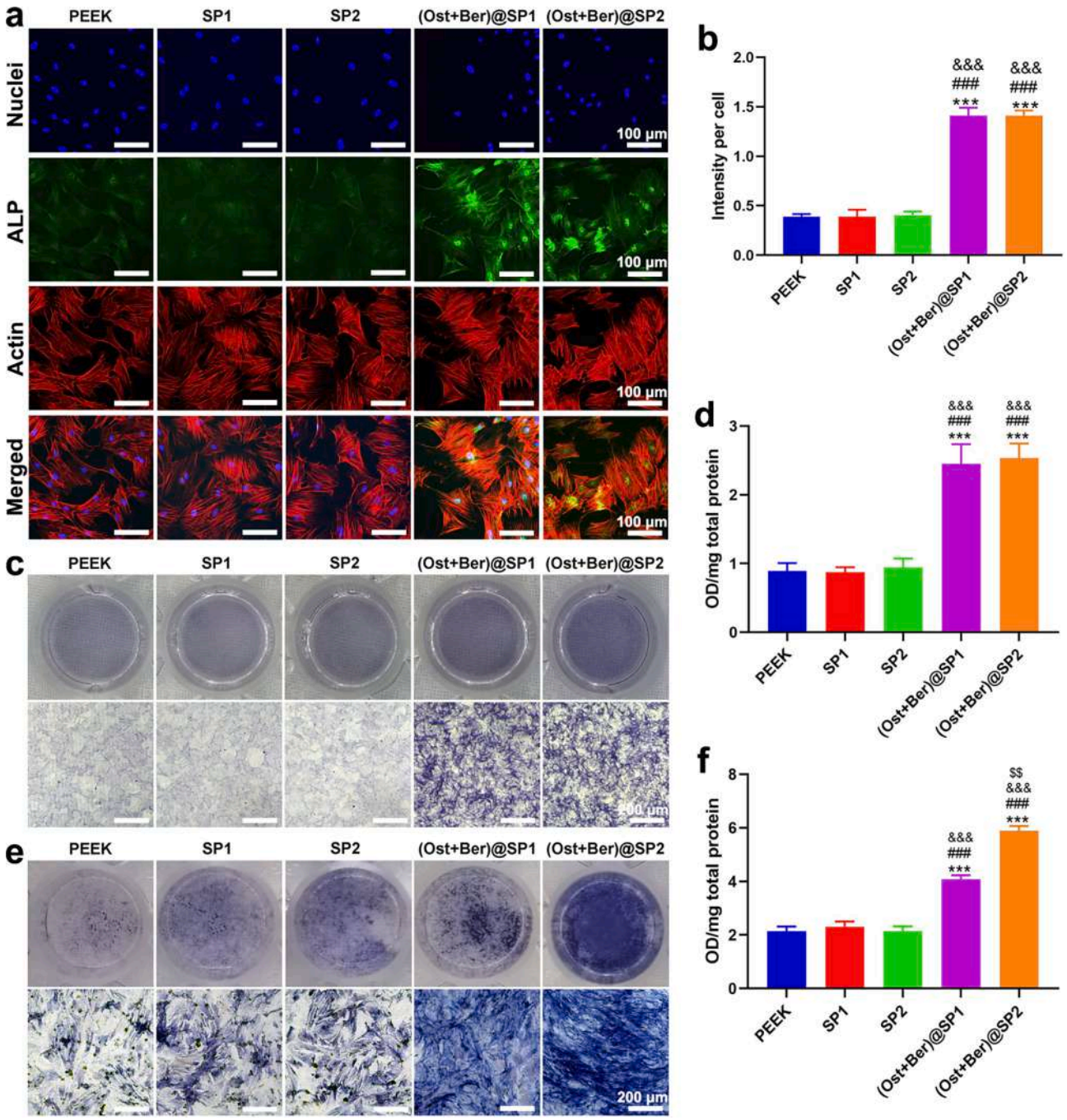

Fig. 4. (a). ALP Immunofluorescence staining of cells on the 7th day of culture. Green (ALP), red (actin), and blue (nuclei). (b). ALP immunofluorescence intensity per cell of the five groups. (c). ALP staining of the five groups of cells on the 7th day of culture; upper images show the whole cell culture pores. (d). ALP activity data in the five groups after 7 days culture. (e). ALP staining of five groups of cells after 14 days culture; upper images show the whole cell culture pores. (f). ALP activity data in the five groups after 14 days of culture. (*, #, & and $ represent the significant differences in statistics when compared with PEEK, SP1, SP2, (Ost + Ber)@SP1 respectively while ***, ### and &&& represent $P < 0.001$, **, ## , &&& and $$ represent $P < 0.01$).

other three groups, whereas they were significantly higher in the (Ost + Ber)@SP2 group than in the (Ost + Ber)@SP1 group. Quantitative analyses of alizarin red staining at 21 days (Fig. 5d) showed similar results to Fig. 4e; (Ost + Ber)@SP2 > (Ost + Ber)@SP1 > PEEK/SP1/SP2. Expression analyses of BMP-2, OCN, and OPN genes in groups on day 14 of culture were performed; osteogenic gene expression in groups showed the following order: (Ost + Ber)@SP2 > (Ost + Ber)@SP1 > PEEK/SP1/SP2 (Fig. 5e–g).

In a word, on the 7th day, the osteogenesis activity intensity of each group was compared as follows: (Ost + Ber)@SP2/(Ost + Ber)@SP1 > PEEK/SP1/SP2. On the 14th day, osteogenesis activity intensity of each group was compared as follows: (Ost + Ber)@SP2 > (Ost + Ber)@SP1 > PEEK/SP1/SP2. On the 21st day, osteogenesis activity intensity of each group was compared as follows: (Ost + Ber)@SP2 > (Ost + Ber)@SP1 > PEEK/SP1/SP2.

3.5. *In vitro anti- Staphylococcus experiments*

Bacteriostatic ring tests for all materials are shown in Fig. 6a and Fig. 6b; bacteriostatic rings were observed around (Ost + Ber)@SP2 and (Ost + Ber)@SP1 wafers, but none for the other groups, suggesting (Ost + Ber)@SP2 and (Ost + Ber)@SP1 exerted bacteriostatic effects against

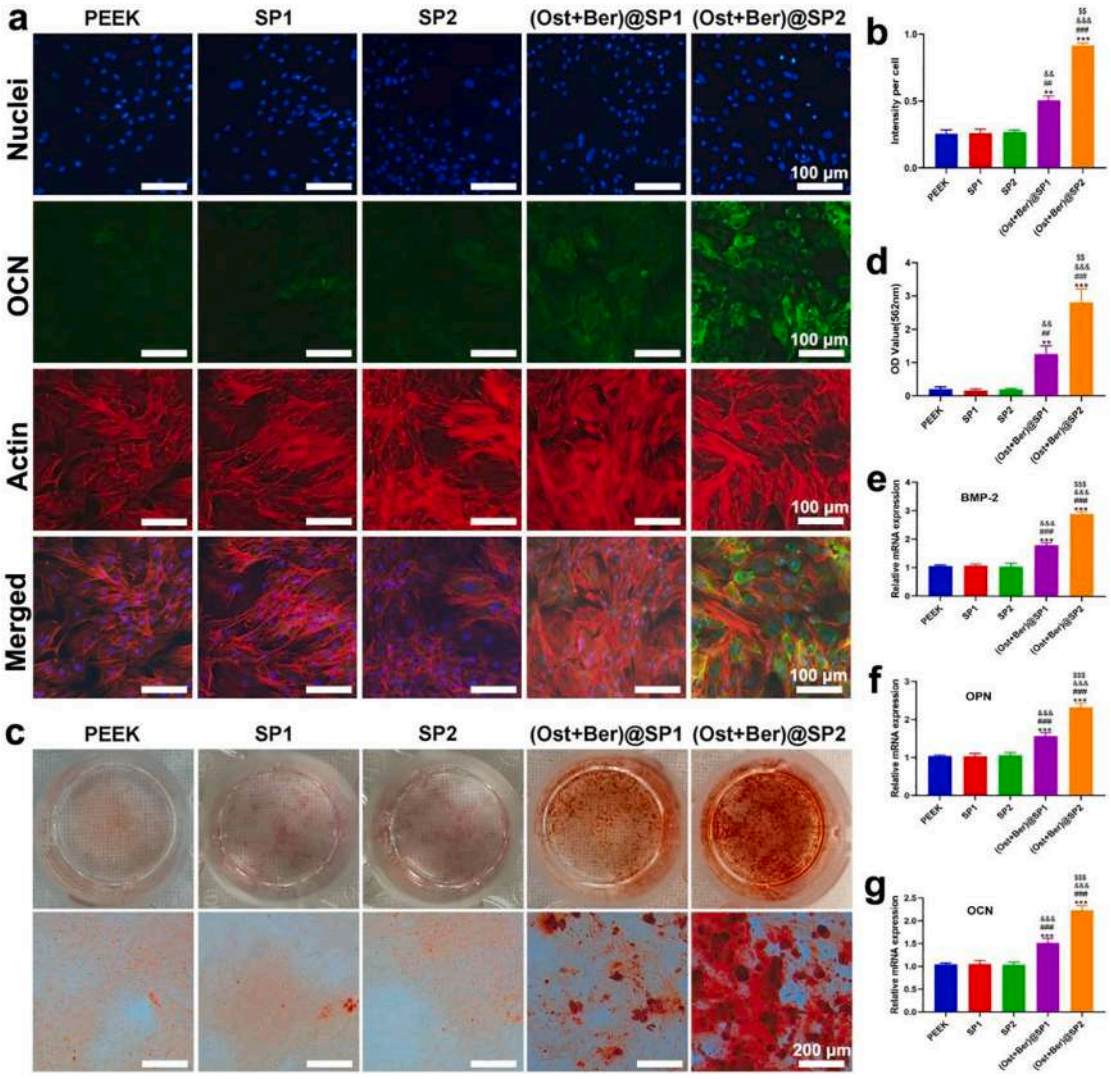

Fig. 5. (a). OCN Immunofluorescence staining of cells on the 14th day of culture. Green (OCN), red (actin), and blue (nuclei). (b). OCN immunofluorescence intensity per cell of the five groups. (c). Alizarin red staining of five groups of cells after 21 days culture; top images show the whole cell culture pores. (d). Quantitative analysis of Alizarin red staining of five groups of cells after 21 days in culture; the image shows an enlarged well. (e–g). Relative expression of the osteogenesis-related genes—BMP-2, OPN, and OCN. (*, #, & and $ represent the significant differences in statistics when compared with PEEK, SP1, SP2, (Ost + Ber)@SP1 respectively while ***, ### and &&& represent $P < 0.001$, **, ## and && represent $P < 0.01$).

S. aureus and *S. epidermidis* growth, whereas the remaining groups exhibited no bacteriostatic effects. Bacterial adhesion to different materials was also demonstrated (Fig. 6i); bacterial numbers in (Ost + Ber)@SP2 and (Ost + Ber)@SP1 groups were significantly lower than the other groups. Fig. 6c, Fig. 6d and Fig. 6e are the results of bacteria adhesion experiment, further confirming that under the same culture conditions, the number of *S. aureus* and *S. epidermidis* attached to the materials of (Ost + Ber)@SP2 and (Ost + Ber)@SP1 groups was significantly less compared with that of the other groups. Fig. 6f, Fig. 6g and Fig. 6h are the results of bacteria-materials co-cultured experiment. These results showed that (Ost + Ber)@SP2 and (Ost + Ber)@SP1 groups exhibited good antibacterial effects toward *S. aureus* and *S. epidermidis* in suspension.

3.6. *In vivo osteogenic experiments*

Fig. 7a showed fewer new bone formation around materials in PEEK, SP1, and SP2 groups both at week 5 and week 10 after implantation. Fig. S13 and Fig. S14 showed the sagittal, coronal and transverse planes images of micro CT of each group of materials and surrounding new bone at week 5 and week 10 after implantation. In contrast, more new bones around (Ost + Ber)@SP2 and (Ost + Ber)@SP1 groups were observed. Moreover, data of Tb.Th, Tb.N, BV/TV, BMD of the new bones around materials are shown in Fig. 7b, Fig. 7c, Fig. 7d and Fig. 7e. The results of these data are: (Ost + Ber)@SP2 > (Ost + Ber)@SP1 > PEEK/SP1/SP2 both at week 5 and week 10 after implantation. VG staining was performed on hard tissue sections in groups of materials at week 10 (Fig. 7f). VG stains bone collagen around materials a red color. The bone collagen content order of the five groups was (Ost + Ber)@SP2 > (Ost + Ber)@SP1 > PEEK/SP1/SP2. Immunofluorescence imaging was performed on tissue sections around the materials (Fig. 7g). Green fluorescence indicated calcein, which reflected new bone formation around the material around the 5th week. New bone content around the five materials around the 5th week was ordered as follows: (Ost + Ber)@SP2 > (Ost + Ber)@SP1 > PEEK/SP1/SP2. The red fluorescence is alizarin red fluorescence, which reflected new bone formation around the material around the 10th week. New bone content around the five materials around the 10th week was ordered as follows: (Ost + Ber)@SP2 > (Ost + Ber)@SP1 > PEEK/SP1/SP2.

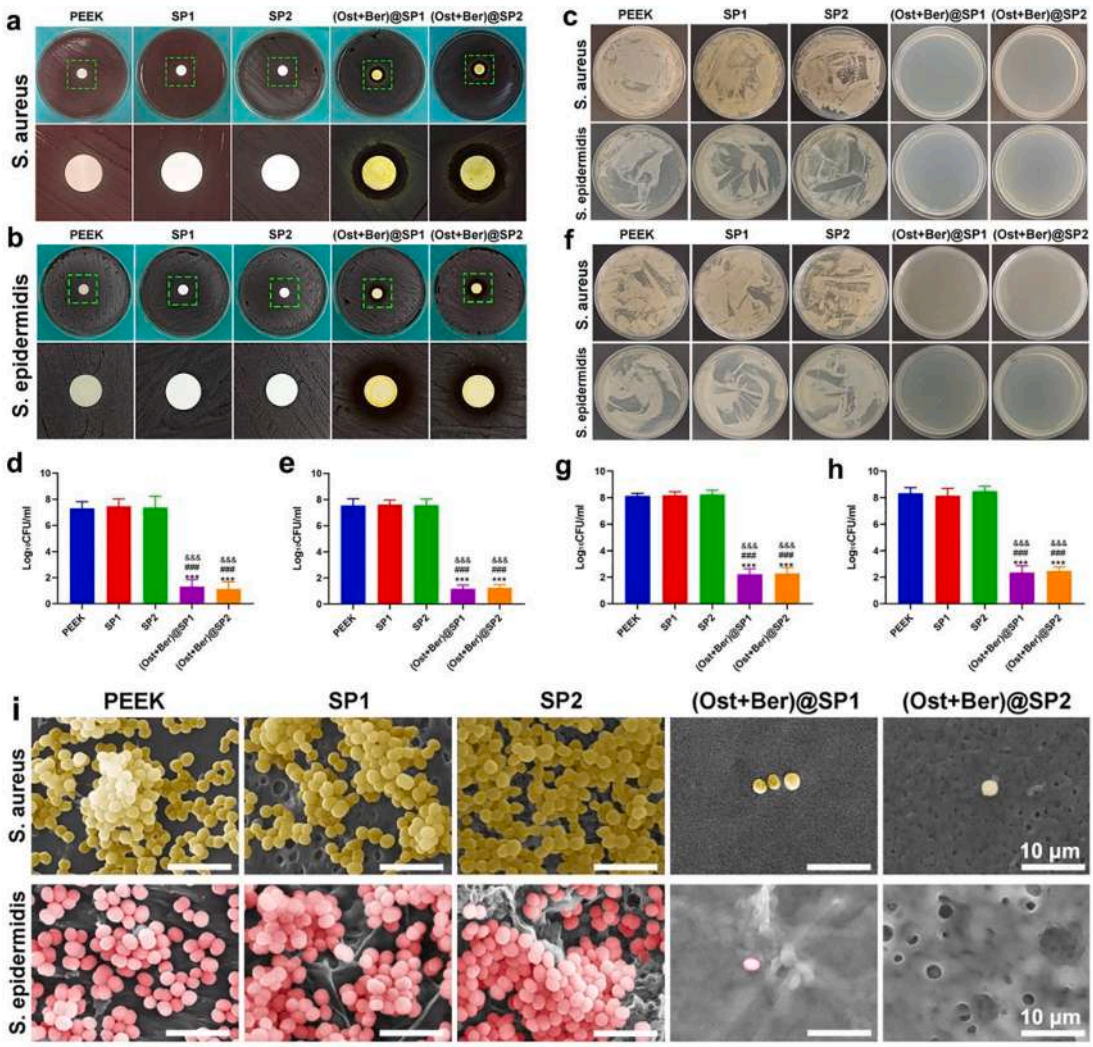

Fig. 6. *In vitro* antibacterial experiments (a). Bacteriostatic ring formation of S. aureus in the five groups. (b). Bacteriostatic ring formation of S. epidermidis in the five groups. (c). Representative culture images of bacterial colonies of each group in bacteria adhesion experiment. (d, e). Statistics of bacterial quantity of S. aureus and S. epidermidis adhesion to the five materials. (f). Representative culture images of bacterial colonies of each group in bacteria adhesion experiment in bacteria-materials co-culture experiment. (g, h). Statistics of bacterial quantity of S. aureus and S. epidermidis co-cultured with five materials (i). SEM images of S. aureus and S. epidermidis adhesion to the five materials. (*, #, & and $ represent the significant differences in statistics when compared with PEEK, SP1, SP2 respectively while ***, ### and &&& represent $P < 0.001$).

3.7. *In vivo anti-infection experiments*

Fig. 8a showed the MRI (T2 weighted imaging) of soft tissue around implants at the end of the 2nd week of implantation. There was obvious edema around implants in PEEK, SP1, and SP2 groups, indicating that the infection around the implants in these groups is very serious at the end of the 2nd week of implantation. Severe bone defects appeared in all of the postoperative femoral condyles in PEEK, SP1, and SP2 groups, suggesting serious osteomyelitis had occurred in these groups five weeks after implantation (Fig. 8b). The postoperative femoral condyle was enveloped by a high degree of inflammatory hyperplastic tissue and implants displacement appeared in all of samples in PEEK, SP1, and SP2 groups. By contrast, in (Ost + Ber)@SP2 and (Ost + Ber)@SP1 groups, inflammation around the implants was mild and all of the implants were in the original location, suggesting no obvious infections (Fig. 8c). HE staining of decalcified bone clearly showed bone destruction around PEEK, SP1, SP2 groups (Fig. 8d). Moreover, inflammatory cells around these materials had proliferated, indicating infection and inflammation around. By contrast, implants in (Ost + Ber)@SP1 and (Ost + Ber)@SP2 groups were tightly wrapped in bone collagen, with almost no inflammatory cell proliferation observed, suggesting no obvious infection and inflammation.

Giemsa staining showed that bacteria levels in PEEK, SP1, and SP2 groups were significantly higher than (Ost + Ber)@SP1 and (Ost + Ber)@SP2 groups, and intuitively revealed the in vivo antibacterial abilities of (Ost + Ber)@SP1 and (Ost + Ber)@SP2 groups (Fig. 8e). Fig. 8f and Fig. S17 showed that bacterial levels around implants in (Ost + Ber)@SP1 and (Ost + Ber)@SP2 groups were significantly lower than those of PEEK, SP1, and SP2 groups. These data indicate that (Ost + Ber)@SP1 and (Ost + Ber)@SP2 groups exhibited good antibacterial activities in vivo.

4. Discussion

Traditional Chinese medicine is a highly valuable Chinese cultural resource and has played a pivotal role in safeguarding the populations' health over centuries [26,27]. However, because of its complex components and uncharacterized active ingredients, its effectiveness has been questioned in the past. Recently, thanks to achievements in modern science, several active ingredients have been purified, with pharmacological effects of single medicines clearly defined [28–33]. In this study, we investigated osthole and berberine and loaded these materials onto

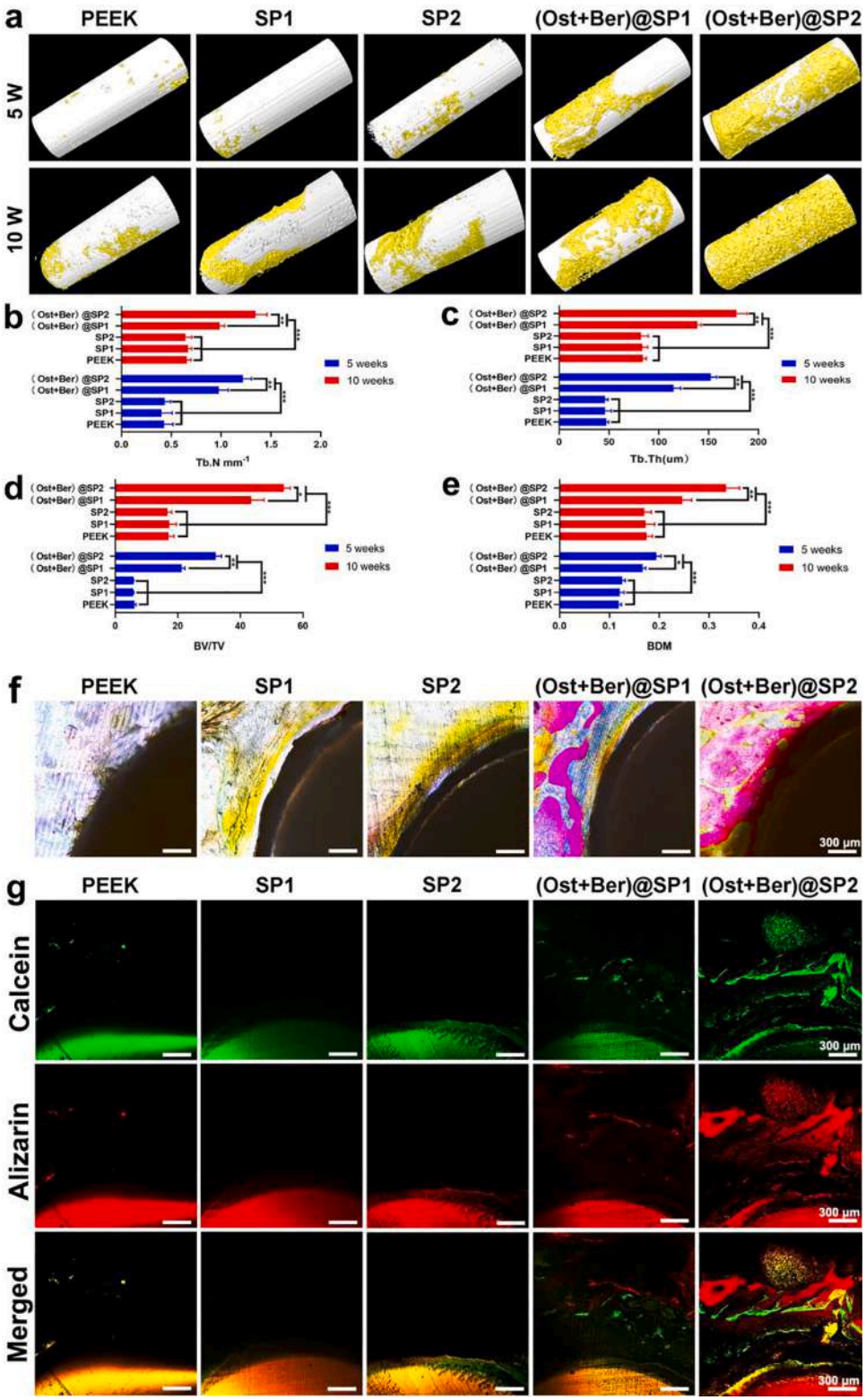

Fig. 7. *In vivo* osteogenic experiments (a). 3D reconstruction images of materials and surrounding new bone at week 5 and week 10 after implantation. (b–e). Tb.Th, Tb.N, BV/TV, and BMD data of bone tissue around materials at week 5 and week 10 after implantation. (* represent statistical differences among different groups while *** represent $P < 0.001$, ** represent $P < 0.01$ and * represent $P < 0.05$) (f). VG staining in hard tissue sections around materials at week 10 of implantation. (g). Calcein and alizarin red fluorescence images of hard tissue sections around materials at week 10 after implantation.

PEEK to investigate their roles in osteogenesis and antibacterial activities.

Osthole is extracted from the Cnidium fruit, which has an important traditional role in promoting osteogenesis [34,35]. Moreover, mechanisms underpinning osthole mediated osteogenesis have been clarified in previous studies [16,19]. However, osthole is poorly soluble in water [18]. Thus, oral or intravenous injections cannot guarantee the effective bioavailability of this molecule. Therefore, to maximize the osteogenic function of osthole, we used a reverse precipitation method to generate osthole nanoparticles and attach osthole to SPEEK using PDA [36]. What's more, we creatively find that the that PDA hinders the crystallization of osthole. In another word, PDA can protect the morphology of osthole nanoparticles. Besides, this method can greatly increase the utilization rate of osthole because osthole nanoparticles can work

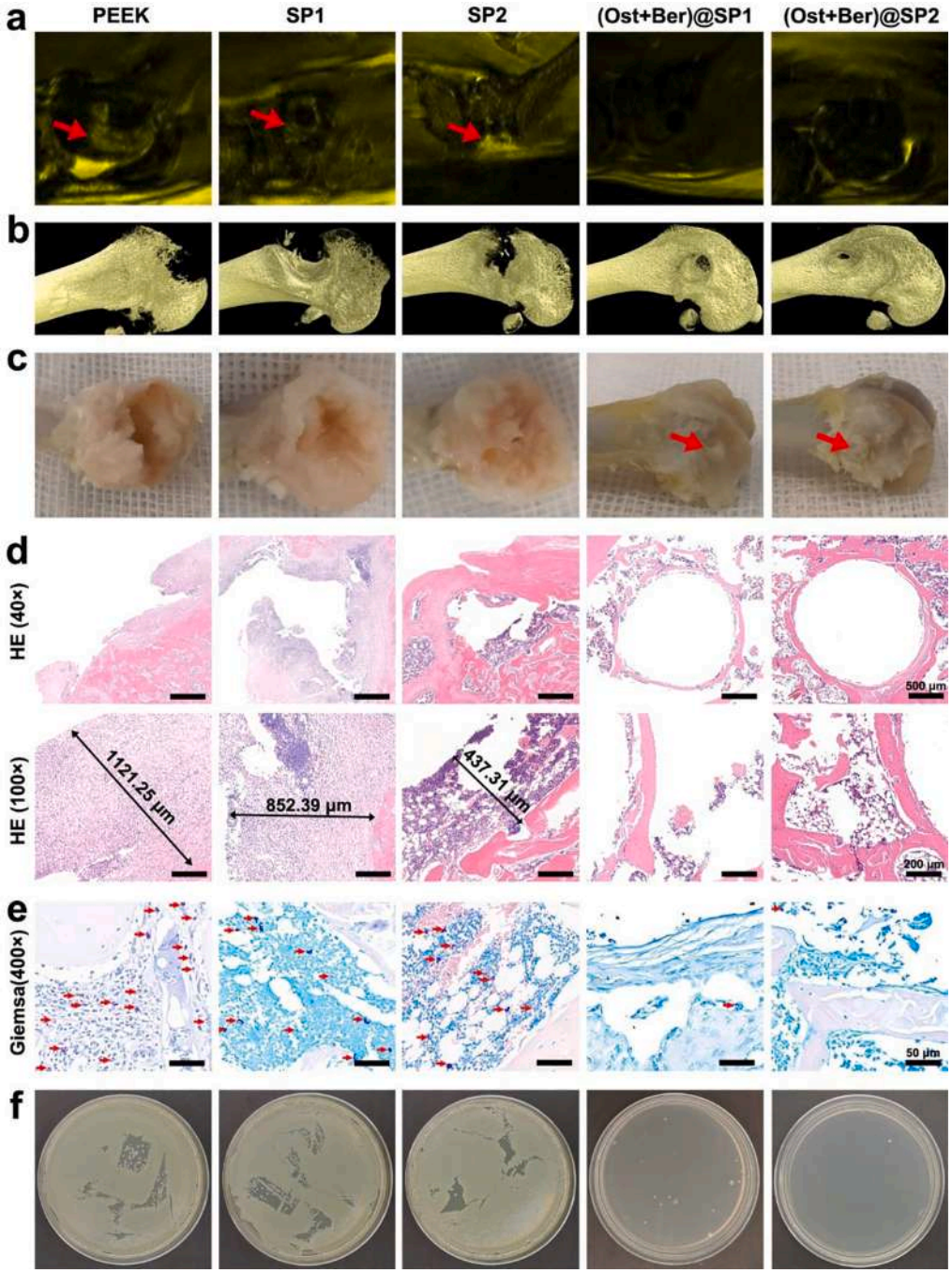

Fig. 8. *In vivo* antibacterial experiments (a). MRI (T2 weighted imaging) of soft tissue around materials at the end of the 2nd week of implantation. The red arrow shows edema around materials. (Images were artificially colored to highlight edema. Raw images are shown in Fig. S15) (b). 3D reconstruction of each group of knee joint at week 5 after implantation (Micro CT images were shown in Fig. S16). (c). Images of postoperative femoral condyle at week 5. The red arrow shows the rod-shaped material. Severe implants displacement appeared in all of the samples from PEEK, SP1, and SP2 groups. (d). Hematoxylin & eosin (HE) and Giemsa staining of pathological sections of decalcified bone around materials 5 weeks after surgery. The red arrow shows S. aureus colonies in tissues. (e). Representative culture images of bacterial colonies of the tissue homogenate around the implants. (Statistics of bacterial quantity of each group were shown in Fig. S17).

directly on osteoblasts at the material-bone interface. The biocompatibility is of vital importance to biomaterials [37,38]. In this experiment, as the total dosage of osthole was very small for each animal used, no side effects were observed in them. (HE staining of pathological sections of major organs in different groups was shown in Fig. S18)

Osseointegration requires a good interface between the prosthesis and bone, with dense new bone around the prosthesis and no gaps between the two [39,40]. Therefore, good bone implant materials should strongly promote osteogenesis and osseointegration [41,42]. However, many studies have reported that PEEK is characterized by poor bone integration [43,44]; therefore, we first loaded osthole nanoparticles on the PEEK surface and endowed it with the ability of osteogenic. Previous studies reported that a porous SPEEK structure could be generated after sulfonation between concentrated sulfuric acid and PEEK [17,45,46]. On this basis, we observed that within a certain time range, with extended reaction times using concentrated sulfuric acid, SPEEK pore sizes became larger, pore numbers increased, and pore distribution became more 3D-like. Moreover, inspired by a sponges ability to absorb water, osthole particles were "absorbed" into the interior of the porous SPEEK.

Our SEM data showed that SP2 "3D-loaded" osthole particles loaded more particles per unit area. Drug release experiments also showed that SP2 loaded with osthole particles in the porous material was more effective compared with SP1 surface loaded osthole particles. Subsequent osteogenesis experiments further confirmed this point. *In vitro* experiments showed that both SP1 and SP2 strongly promoted osteoblast differentiation during the early stages (1 week), with no significant differences between groups, consistent with drug release tests; in 1 week, both SP1 and SP2 groups stably released osthole, with little difference in osthole release rates between the groups. At 2 and 3 weeks,

although both (Ost + Ber)@SP1 and (Ost + Ber)@SP2 promoted osteoblast differentiation, the osteogenic effects in the (Ost + Ber)@SP2 group were significantly stronger than the (Ost + Ber)@SP1 group. This was because the osthole release rate of the (Ost + Ber)@SP1 group gradually decreased 1 week later, so its osteogenic effects gradually weakened. The (Ost + Ber)@SP2 group steadily released osthole during the 4-week drug release experiment; thus, its osteogenic effects were the strongest and long-lasting. The experimental results in vivo also support this conclusion. Regardless of 5 or 10 weeks, the (Ost + Ber)@SP2 group strongly promoted osteogenesis and osseointegration in vivo. (Ost + Ber)@SP2 displayed the best effects in promoting osteogenesis both in vivo and *in vitro*. Thus, our experiments proved that (Ost + Ber)@SP2, with a porous spongy structure, exhibited the strongest and most stable osteogenic effects.

In some cases, infection after joint replacement may be a catastrophic consequence for patients undergoing joint replacement [47–50]. In addition, some patients who undergo revision surgery may acquire another infection after the operation. The root cause of this issue is attributed to the fact current prostheses do no exert antibacterial qualities [51,52]. As a potential novel joint prosthesis material, PEEK or SPEEK both exert no antibacterial capabilities. It was reported that a large amount of joint prosthesis infections are caused by *Staphylococcus* [53,54]. Based on this information, berberine, which exhibits strong bactericidal effects against *Staphylococcus*, was loaded onto PEEK and endowed it with antibacterial functions [55]. Clinically, the peak of infection after joint prosthesis surgery occurs within 3 days post operation [56,57]. For patients with a joint prosthesis infection or a high risk of infection, antibiotics are often mixed into bone cement during surgery, or large antibiotic doses are intravenously infused [58,59]. To some extent, adding antibiotics to bone cement can effectively prevents infection, but antibiotics are released too quickly, with large doses of intravenous antibiotics potentially causing liver and kidney damage [60,61]. In this study, we used silk protein to load berberine. Silk protein coating can significantly improve SPEEK hydrophilicity, so when the material is immersed in berberine solution, the physical loading of berberine to the material increased. More importantly, silk protein is rich in carboxyl groups, which covalently adsorb berberine containing quaternary ammonia bonds [23]. The dual effects of physical and chemical adsorption increase berberine loading and promotes a rapid and sustained berberine release. Our drug release curve analyses showed that (Ost + Ber)@SP1 and (Ost + Ber)@SP2 released berberine rapidly in the first 4 h, whereas it was sustainedly released during the next 72 h. This drug release characteristic is consistent with the clinical use of antimicrobials [62]; large doses are initially used, with stable concentrations maintained in follow-up treatments. It is worth noting that the use of antimicrobials does not mean the longer you use them, the better the effect, as the prolonged antibiotic use will lead to drug-resistant bacteria [63,64]. Likewise, berberine release from our materials does not violate this principle. Subsequent *in vitro* antibacterial experiments showed that berberine loaded with (Ost + Ber)@SP1 and (Ost + Ber)@SP2 effectively prevented *Staphylococcus* adhesion, but also exerted strong bactericidal effects on *Staphylococcus* suspensions. *In vivo* experiments proved that rod-shaped (Ost + Ber)@SP1 and (Ost + Ber)@SP2 effectively prevented periprosthetic infection caused by *Staphylococcus*. Thus, (Ost + Ber)@SP1 and (Ost + Ber)@SP2 effectively killed *Staphylococcus in vitro* and in vivo and prevented implant-related infections around the prosthesis.

5. Conclusion

In summary, we loaded osthole and berberine onto the SPEEK surface, facilitating osteogenic and antibacterial capabilities. Our research not only provides a new direction for the production of bioactive orthopedic biomaterials but also opens up new pathways for the application of traditional Chinese medicine in modern clinical settings.

Declaration of Competing Interest

The authors declare that they have no known competing financial interests or personal relationships that could have appeared to influence the work reported in this paper.

Acknowledgements

This research was supported by the National Natural Science Foundation of China (81974324, 81772309) and Shanghai Sailing Program (21YF1433800).

Appendix A. Supplementary data

Supplementary data to this article can be found online at https://doi.org/10.1016/j.cej.2022.135255.

References

[1] R.J. Ferguson, A.J.R. Palmer, A. Taylor, M.L. Porter, H. Malchau, S. Glyn-Jones, Hip replacement, The Lancet 392 (10158) (2018) 1662–1671, https://doi.org/10.1016/s0140-6736(18)31777-x.
[2] A.J. Price, A. Alvand, A. Troelsen, J.N. Katz, G. Hooper, A. Gray, A. Carr, D. Beard, Knee replacement, The Lancet 392 (10158) (2018) 1672–1682, https://doi.org/10.1016/s0140-6736(18)32344-4.
[3] M. Nugent, S.W. Young, C.M. Frampton, G.J. Hooper, The lifetime risk of revision following total hip arthroplasty: a New Zealand Joint Registry study, The Bone & Joint J. 103-B (3) (2021) 479–485.
[4] A. El-Galaly, A. Kappel, P.T. Nielsen, S.L. Jensen, Revision risk for total knee arthroplasty converted from medial unicompartmental knee arthroplasty: comparison with primary and revision arthroplasties, based on mid-term results from the danish knee arthroplasty registry, J. Bone Joint Surgery American 101 (22) (2019) 1999–2006, https://doi.org/10.2106/JBJS.18.01468.
[5] L. Bernard, C. Arvieux, B. Brunschweiler, S. Touchais, S. Ansart, J.P. Bru, E. Oziol, C. Boeri, G. Gras, J. Druon, P. Rosset, E. Senneville, H. Bentayeb, D. Bouhour, G. Le Moal, J. Michon, H. Aumaitre, E. Forestier, J.M. Laffosse, T. Begue, C. Chirouze, F. A. Dauchy, E. Devaud, B. Martha, D. Burgot, D. Boutoille, E. Stindel, A. Dinh, P. Bemer, B. Giraudeau, B. Issartel, A. Caille, Antibiotic Therapy for 6 or 12 Weeks for Prosthetic Joint Infection, New Engl. J. Med. 384 (21) (2021) 1991–2001, https://doi.org/10.1056/NEJMoa2020198Copyright<(c)>2021MassachusettsMedicalSociety.
[6] M.C. Weiser, C.S. Moucha, The Current State of Screening and Decolonization for the Prevention of Staphylococcus aureus Surgical Site Infection After Total Hip and Knee Arthroplasty, J. Bone Joint Surgery American 97 (17) (2015) 1449–1458, https://doi.org/10.2106/JBJS.N.01114.
[7] A.W. Burns, R.B. Bourne, B.M. Chesworth, S.J. MacDonald, C.H. Rorabeck, Cost effectiveness of revision total knee arthroplasty, Clinical Orthopaedics Related Res. 446 (2006) 29–33, https://doi.org/10.1097/01.blo.0000214420.14088.76.
[8] K.J. Bozic, S.M. Kurtz, E. Lau, K. Ong, T.P. Vail, D.J. Berry, The epidemiology of revision total hip arthroplasty in the United States, J. Bone Joint Surgery American 91 (1) (2009) 128–133, https://doi.org/10.2106/JBJS.H.00155.
[9] S.M. Kurtz, J.N. Devine, PEEK biomaterials in trauma, orthopedic, and spinal implants, Biomaterials 28 (32) (2007) 4845–4869, https://doi.org/10.1016/j.biomaterials.2007.07.013.
[10] F.B. Torstrick, N.T. Evans, H.Y. Stevens, K. Gall, R.E. Guldberg, Do Surface Porosity and Pore Size Influence Mechanical Properties and Cellular Response to PEEK? Clinical Orthopaedics Related Research 474 (11) (2016) 2373–2383, https://doi.org/10.1007/s11999-016-4833-0.
[11] B. Chen, H. Xiang, S. Pan, L. Yu, T. Xu, Y.u. Chen, Advanced Theragenerative Biomaterials with Therapeutic and Regeneration Multifunctionality, Advanced Functional Materials 30 (34) (2020) 2002621, https://doi.org/10.1002/adfm.202002621.
[12] J. Min, K.Y. Choi, E.C. Dreaden, R.F. Padera, R.D. Braatz, M. Spector, P. T. Hammond, Designer Dual Therapy Nanolayered Implant Coatings Eradicate Biofilms and Accelerate Bone Tissue Repair, ACS nano 10 (4) (2016) 4441–4450, https://doi.org/10.1021/acsnano.6b0008710.1021/acsnano.6b00087.s001.
[13] S. Mo, F. Zhao, A. Gao, Y. Wu, Q. Liao, L. Xie, H. Pan, L. Tong, P.K. Chu, H. Wang, Simultaneous application of diamond-like carbon coating and surface amination on polyether ether ketone: Towards superior mechanical performance and osseointegration, Smart Materials in Medicine 2 (2021) 219–228, https://doi.org/10.1016/j.smaim.2021.07.004.
[14] A. Gao, Q. Liao, L. Xie, G. Wang, W. Zhang, Y. Wu, P. Li, M. Guan, H. Pan, L. Tong, P.K. Chu, H. Wang, Tuning the surface immunomodulatory functions of polyetheretherketone for enhanced osseointegration, Biomaterials 230 (2020) 119642, https://doi.org/10.1016/j.biomaterials.2019.119642.
[15] H. Yu, D. Zhu, P. Liu, Q. Yang, J. Gao, Y. Huang, Y. Chen, Y. Gao, C. Zhang, Osthole stimulates bone formation, drives vascularization and retards adipogenesis to alleviate alcohol-induced osteonecrosis of the femoral head, J Cell Mol Med 24 (8) (2020) 4439–4451, https://doi.org/10.1111/jcmm.15103.

[16] D.-Z. Tang, W. Hou, Q. Zhou, M. Zhang, J. Holz, T.-J. Sheu, T.-F. Li, S.-D. Cheng, Q. Shi, S.E. Harris, D. Chen, Y.-J. Wang, Osthole stimulates osteoblast differentiation and bone formation by activation of β-catenin-BMP signaling, Journal of Bone and Mineral Research 25 (6) (2010) 1234–1245, https://doi.org/10.1002/jbmr.21.

[17] Y. Zhao, H.M. Wong, W. Wang, P. Li, Z. Xu, E.Y. Chong, C.H. Yan, K.W. Yeung, P. K. Chu, Cytocompatibility, osseointegration, and bioactivity of three-dimensional porous and nanostructured network on polyetheretherketone, Biomaterials 34 (37) (2013) 9264–9277, https://doi.org/10.1016/j.biomaterials.2013.08.071.

[18] R. Wang, Y.Y. Liu, X. Hu, J.H. Pan, D.M. Gong, G.W. Zhang, New insights into the binding mechanism between osthole and beta-lactoglobulin: Spectroscopic, chemometrics and docking studies, Food Res Int 120 (2019) 226–234, https://doi.org/10.1016/j.foodres.2019.02.042.

[19] Z.X. Jin, X.Y. Liao, W.W. Da, Y.J. Zhao, X.F. Li, D.Z. Tang, Osthole enhances the bone mass of senile osteoporosis and stimulates the expression of osteoprotegerin by activating beta-catenin signaling, Stem cell research & therapy 12 (1) (2021) 154, https://doi.org/10.1186/s13287-021-02228-6.

[20] L. Kokoska, P. Kloucek, O. Leuner, P. Novy, Plant-Derived Products as Antibacterial and Antifungal Agents in Human Health Care, Current medicinal chemistry 26 (29) (2019) 5501–5541, https://doi.org/10.2174/0929867325666180831144344.

[21] L. Peng, S. Kang, Z. Yin, R. Jia, X. Song, L. Li, Z. Li, Y. Zou, X. Liang, L. Li, C. He, G. Ye, L. Yin, F. Shi, C. Lv, B. Jing, Antibacterial activity and mechanism of berberine against Streptococcus agalactiae, International journal of clinical and experimental pathology 8 (5) (2015) 5217–5223.

[22] S. Kang, Z. Li, Z. Yin, R. Jia, X. Song, L. Li, Z. Chen, L. Peng, J. Qu, Z. Hu, X. Lai, G. Wang, X. Liang, C. He, L. Yin, The antibacterial mechanism of berberine against Actinobacillus pleuropneumoniae, Natural product research 29 (23) (2015) 2203–2206, https://doi.org/10.1080/14786419.2014.1001388.

[23] Y.e. Tian, X. Jiang, X. Chen, Z. Shao, W. Yang, Doxorubicin-loaded magnetic silk fibroin nanoparticles for targeted therapy of multidrug-resistant cancer, Advanced materials 26 (43) (2014) 7393–7398, https://doi.org/10.1002/adma.201403562.

[24] D.N. Rockwood, R.C. Preda, T. Yucel, X. Wang, M.L. Lovett, D.L. Kaplan, Materials fabrication from Bombyx mori silk fibroin, Nature protocols 6 (10) (2011) 1612–1631, https://doi.org/10.1038/nprot.2011.379.

[25] P. Xia, H.-Y. Chen, S.-F. Chen, L. Wang, P.M. Strappe, H.-l. Yang, C.-H. Zhou, X. Zhang, Y.-X. Zhang, L.-l. Ma, L. Wang, The stimulatory effects of eNOS/F92A-Cav1, Biomedicine & Pharmacotherapy 77 (2016) 7–13, https://doi.org/10.1016/j.biopha.2015.11.001.

[26] A.A. Skolnick, Old Chinese herbal medicine used for fever yields possible new Alzheimer disease therapy, JAMA 277 (10) (1997) 776, https://doi.org/10.1001/jama.1997.03540340010004.

[27] A. Bensoussan, N.J. Talley, M. Hing, R. Menzies, A. Guo, M. Ngu, Treatment of irritable bowel syndrome with Chinese herbal medicine: a randomized controlled trial, JAMA 280 (18) (1998) 1585–1589, https://doi.org/10.1001/jama.280.18.1585.

[28] P. Zheng, B. Ding, R. Shi, Z. Jiang, W. Xu, G. Li, J. Ding, X. Chen, A Multichannel Ca(2+) Nanomodulator for Multilevel Mitochondrial Destruction-Mediated Cancer Therapy, Advanced materials 33 (15) (2021) 2007426, https://doi.org/10.1002/adma.202007426.

[29] J. Zhang, L. Shen, X. Li, W. Song, Y. Liu, L. Huang, Nanoformulated codelivery of quercetin and alantolactone promotes an antitumor response through synergistic immunogenic cell death for microsatellite-stable colorectal cancer, ACS nano 13 (11) (2019) 12511–12524, https://doi.org/10.1021/acsnano.9b0287510.1021/acsnano.9b02875.s001.

[30] G. Jin, M.P. Prabhakaran, D. Kai, S.K. Annamalai, K.D. Arunachalam, S. Ramakrishna, Tissue engineered plant extracts as nanofibrous wound dressing, Biomaterials 34 (3) (2013) 724–734, https://doi.org/10.1016/j.biomaterials.2012.10.026.

[31] J. Chi, L. Sun, L. Cai, L. Fan, C. Shao, L. Shang, Y. Zhao, Chinese herb microneedle patch for wound healing, Bioactive materials 6 (10) (2021) 3507–3514, https://doi.org/10.1016/j.bioactmat.2021.03.023.

[32] L. Yang, C. Zhan, X. Huang, L. Hong, L. Fang, W. Wang, J. Su, Durable Antibacterial Cotton Fabrics Based on Natural Borneol-Derived Anti-MRSA Agents, Advanced healthcare materials 9 (11) (2020) 2000186, https://doi.org/10.1002/adhm.202000186.

[33] H. Tang, A. Hosein, M. Mattioli-Belmonte, Traditional Chinese Medicine and orthopedic biomaterials: Host of opportunities from herbal extracts, Materials science & engineering, C, Materials for biological applications 120 (2021) 111760, https://doi.org/10.1016/j.msec.2020.111760.

[34] M. Waqas, Y. Wang, A. Li, H. Qamar, W. Yao, X. Tong, J. Zhang, M. Iqbal, K. Mehmood, J. Li, Osthole: A Coumarin Derivative Assuage Thiram-Induced Tibial Dyschondroplasia by Regulating BMP-2 and RUNX-2 Expressions in Chickens, Antioxidants 8 (9) (2019) 330, https://doi.org/10.3390/antiox8090330.

[35] Z.-R. Zhang, W. Leung, G. Li, S. Kong, X. Lu, Y. Wong, C. Chan, Osthole Enhances Osteogenesis in Osteoblasts by Elevating Transcription Factor Osterix via cAMP/CREB Signaling In Vitro and In Vivo, Nutrients 9 (6) (2017) 588, https://doi.org/10.3390/nu9060588.

[36] L.i. Huang, S. Zhao, F. Fang, T. Xu, M. Lan, J. Zhang, Advances and perspectives in carrier-free nanodrugs for cancer chemo-monotherapy and combination therapy, Biomaterials 268 (2021) 120557, https://doi.org/10.1016/j.biomaterials.2020.120557.

[37] W.-Y. Chen, X.-L. Shi, J. Zou, Z.-G. Chen, Wearable fiber-based thermoelectrics from materials to applications, NANO Energy 81 (2021) 105684, https://doi.org/10.1016/j.nanoen.2020.105684.

[38] R. Ettlinger, U. Lachelt, R. Gref, P. Horcajada, T. Lammers, C. Serre, P. Couvreur, R. E. Morris, S. Wuttke, Toxicity of metal-organic framework nanoparticles: from essential analyses to potential applications, Chem Soc Rev 51 (2) (2022) 464–484, https://doi.org/10.1039/d1cs00918d.

[39] C. Hu, D. Ashok, D.R. Nisbet, V. Gautam, Bioinspired surface modification of orthopedic implants for bone tissue engineering, Biomaterials 219 (2019) 119366, https://doi.org/10.1016/j.biomaterials.2019.119366.

[40] R. Agarwal, C. Gonzalez-Garcia, B. Torstrick, R.E. Guldberg, M. Salmeron-Sanchez, A.J. Garcia, Simple coating with fibronectin fragment enhances stainless steel screw osseointegration in healthy and osteoporotic rats, Biomaterials 63 (2015) 137–145, https://doi.org/10.1016/j.biomaterials.2015.06.025.

[41] Y.i. Deng, S. Wei, L. Yang, W. Yang, M.S. Dargusch, Z.-G. Chen, A Novel Hydrogel Surface Grafted With Dual Functional Peptides for Sustaining Long-Term Self-Renewal of Human Induced Pluripotent Stem Cells and Manipulating Their Osteoblastic Maturation, Advanced Functional Materials 28 (11) (2018) 1705546, https://doi.org/10.1002/adfm.201705546.

[42] L. Xie, G. Wang, Y. Wu, Q. Liao, S. Mo, X. Ren, L. Tong, W. Zhang, M. Guan, H. Pan, P.K. Chu, H. Wang, Programmed surface on poly(aryl-ether-ether-ketone) initiating immune mediation and fulfilling bone regeneration sequentially, Innovation (N Y) 2 (3) (2021) 100148, https://doi.org/10.1016/j.xinn.2021.100148.

[43] F.B. Torstrick, A.S.P. Lin, D. Potter, D.L. Safranski, T.A. Sulchek, K. Gall, R. E. Guldberg, Porous PEEK improves the bone-implant interface compared to plasma-sprayed titanium coating on PEEK, Biomaterials 185 (2018) 106–116, https://doi.org/10.1016/j.biomaterials.2018.09.009.

[44] S. Huo, F. Wang, Z. Lyu, Q. Hong, B. Nie, J. Wei, Y. Wang, J. Zhang, B. Yue, Dual-functional polyetheretherketone surface modification for regulating immunity and bone metabolism, Chemical Engineering Journal 426 426 (2021) 130806, https://doi.org/10.1016/j.cej.2021.130806.

[45] J. Zhang, X. Gao, D. Ma, S. He, B. Du, W. Yang, K. Xie, L.u. Xie, Y.i. Deng, Copper ferrite heterojunction coatings empower polyetheretherketone implant with multi-modal bactericidal functions and boosted osteogenicity through synergistic photo/Fenton-therapy, Chemical Engineering Journal 422 (2021) 130094, https://doi.org/10.1016/j.cej.2021.130094.

[46] Y.i. Deng, X. Gao, X.-L. Shi, S. Lu, W. Yang, C. Duan, Z.-G. Chen, Graphene Oxide and Adiponectin-Functionalized Sulfonated Poly(etheretherketone) with Effective Osteogenicity and Remotely Repeatable Photodisinfection, Chemistry of Materials 32 (5) (2020) 2180–2193, https://doi.org/10.1021/acs.chemmater.0c0029010.1021/acs.chemmater.0c00290.s001.

[47] W. Zimmerli, A.F. Widmer, M. Blatter, R. Frei, P.E. Ochsner, Role of rifampin for treatment of orthopedic implant-related staphylococcal infections: a randomized controlled trial, Foreign-Body Infection (FBI) Study Group, Jama 279(19) (1998) 1537–1541, https://doi.org/10.1001/jama.279.19.1537.

[48] J.L. Del Pozo, R. Patel, Clinical practice, Infection associated with prosthetic joints, The New England journal of medicine 361 (8) (2009) 787–794, https://doi.org/10.1056/NEJMcp0905029.

[49] G. Labek, M. Thaler, W. Janda, M. Agreiter, B. Stockl, Revision rates after total joint replacement: cumulative results from worldwide joint register datasets, The Journal of bone and joint surgery, British 93 (3) (2011) 293–297, https://doi.org/10.1302/0301-620X.93B3.25467.

[50] S. Kurtz, K. Ong, E. Lau, F. Mowat, M. Halpern, Projections of primary and revision hip and knee arthroplasty in the United States from 2005 to 2030, The Journal of bone and joint surgery, American 89 (4) (2007) 780–785, https://doi.org/10.2106/JBJS.F.00222.

[51] X. Xu, Y.L. Li, L.X. Wang, Y. Li, J.J. Pan, X.M. Fu, Z.Y. Luo, Y. Sui, S.Q. Zhang, L. Wang, Y.F. Ni, L. Zhang, S.C. Wei, Triple-functional polyetheretherketone surface with enhanced bacteriostasis and anti-inflammatory and osseointegrative properties for implant application, Biomaterials 212 (2019) 98–114, https://doi.org/10.1016/j.biomaterials.2019.05.014.

[52] J. Yan, W. Zhou, Z. Jia, P. Xiong, Y. Li, P. Wang, Q. Li, Y. Cheng, Y. Zheng, Endowing polyetheretherketone with synergistic bactericidal effects and improved osteogenic ability, Acta biomaterialia 79 (2018) 216–229, https://doi.org/10.1016/j.actbio.2018.08.037.

[53] W. Zimmerli, A. Trampuz, P.E. Ochsner, Prosthetic-joint infections, The New England journal of medicine 351 (16) (2004) 1645–1654, https://doi.org/10.1056/NEJMra040181.

[54] F.D. Lowy, Staphylococcus aureus infections, The New England journal of medicine 339 (8) (1998) 520–532, https://doi.org/10.1056/NEJM199808203390806.

[55] X.M. Huang, P.L. Wang, T. Li, X.H. Tian, W.B. Guo, B. Xu, G.R. Huang, D.S. Cai, F. Zhou, H. Zhang, H.M. Lei, Self-Assemblies Based on Traditional Medicine Berberine and Cinnamic Acid for Adhesion-Induced Inhibition Multidrug-Resistant Staphylococcus aureus, ACS applied materials & interfaces 12 (1) (2020) 227–237, https://doi.org/10.1021/acsami.9b17722.

[56] P.M. Dohmen, Antibiotic resistance in common pathogens reinforces the need to minimise surgical site infections, The Journal of hospital infection 70 (Suppl 2) (2008) 15–20, https://doi.org/10.1016/S0195-6701(08)60019-5.

[57] P. Bedouch, J. Labarere, E. Chirpaz, B. Allenet, A. Lepape, M. Fourny, P. Pavese, P. Girardet, P. Merloz, D. Saragaglia, J. Calop, P. Francois, Compliance with guidelines on antibiotic prophylaxis in total hip replacement surgery: results of a retrospective study of 416 patients in a teaching hospital, Infection control and hospital epidemiology 25 (4) (2004) 302–307, https://doi.org/10.1086/502396.

[58] J. Slane, B. Gietman, M. Squire, Antibiotic elution from acrylic bone cement loaded with high doses of tobramycin and vancomycin, Journal of orthopaedic research : official publication of the Orthopaedic Research Society 36 (4) (2018) 1078–1085, https://doi.org/10.1002/jor.23722.

[59] Z.C. Liang, C. Yang, X. Ding, J.L. Hedrick, W. Wang, Y.Y. Yang, Carboxylic acid-functionalized polycarbonates as bone cement additives for enhanced and sustained release of antibiotics, Journal of controlled release : official journal of the

Controlled Release Society 329 (2021) 871–881, https://doi.org/10.1016/j.jconrel.2020.10.018.
[60] V. Antoci Jr., C.S. Adams, N.J. Hickok, I.M. Shapiro, J. Parvizi, Antibiotics for local delivery systems cause skeletal cell toxicity in vitro, Clinical orthopaedics and related research 462 (2007) 200–206, https://doi.org/10.1097/BLO.0b013e31811ff866.
[61] E. Prina, O.T. Ranzani, A. Torres, Community-acquired pneumonia, Lancet 386 (9998) (2015) 1097–1108, https://doi.org/10.1016/S0140-6736(15)60733-4.
[62] N.J. Onufrak, A. Forrest, D. Gonzalez, Pharmacokinetic and Pharmacodynamic Principles of Anti-infective Dosing, Clin Ther 38 (9) (2016) 1930–1947, https://doi.org/10.1016/j.clinthera.2016.06.015.
[63] H. McCarthy, J.K. Rudkin, N.S. Black, L. Gallagher, E. O'Neill, J.P. O'Gara, Methicillin resistance and the biofilm phenotype in Staphylococcus aureus, Frontiers in cellular and infection microbiology 5 (2015) 1, https://doi.org/10.3389/fcimb.2015.00001.
[64] D.I. Andersson, D. Hughes, Evolution of antibiotic resistance at non-lethal drug concentrations, Drug Resist Update 15 (3) (2012) 162–172, https://doi.org/10.1016/j.drup.2012.03.005.